Applied Energy 211 (2018) 843–853

Contents lists available at ScienceDirect

Applied Energy

journal homepage: www.elsevier.com/locate/apenergy

Performance assessment of catalytic combustion-driven thermophotovoltaic platinum tubular reactor☆

Yueh-Heng Li*, Jing-Ru Hong

Department of Aeronautics and Astronautics, National Cheng Kung University, Tainan 701, Taiwan, ROC

HIGHLIGHTS

- H_2 is injected in the inner tube to assist CH_4 catalytic combustion in the outer tube.
- The prototype TPV system comprises the micro-TPV reactor with GaSb PV cell array.
- Radiant efficient of a metal oxide–deposited quartz tube is behind the expectation.
- The system with a recirculating cap and a reflecting mirror are employed.
- The overall efficiency of the micro TPV system is measured under various conditions.

ARTICLE INFO

Keywords:
Catalytic combustion
Platinum
Small-scale reactor
Heterogeneous and homogenous reaction
Thermophotovoltaic

ABSTRACT

This study is aimed to enhance the overall efficiency of micro-thermophotovoltaic (micro-TPV) reactor by collecting radiations from emitter and combustion chamber. However, the proper fuel deployment and fluid design for the micro-TPV reactor are strongly associated with combustion stability and radiant intensity of the micro-TPV reactor. Therefore, the system performance of the micro-TPV reactor was investigated with regard to combustion, thermal radiation, and electrical output. A platinum tube with a ring of perforated holes was utilised with specific fuel deployment, that is, hydrogen employed in the inner chamber for facilitating induction of methane catalytic combustion in the outer chamber. Because of the inherently high diffusivity of hydrogen, the heat and radicals could be delivered to the other chamber through the perforated holes; in this manner, the methane catalytic combustion could be successfully initiated. The flame-stabilizing mechanism of micro-TPV platinum tubular reactor was addressed and interpreted through the simplified simulation of segmented platinum tubular reactor with a gap. The effective power efficiency of the TPV system was 3.24% when $ER_{in\text{-}H_2} = 0.7$ and $ER_{out\text{-}CH_4} = 0.9$. With a mirror and a recirculating tube, effective power efficiency was enhanced to 6.32%.

1. Introduction

With the rapid development of electrically powered devices, the need for portable power systems is steadily growing. Electrically powered vehicles, unmanned aerial vehicles (UAV), and unmanned submarines exemplify the importance of power systems that deliver electricity with low noise and high reliability [1]. Long-endurance reconnaissance drones have been developed and can be applied in security and monitoring situations that require persistent flight, such as aerial reconnaissance, border patrol, forest fire observation, and battlefield management. A solar-powered UAV travelled 336 h continuously; electric UAVs can fly at stratospheric altitudes all over the world, and have wide-area military and civil potential, because they offer capabilities far beyond those of existing satellites and aircraft. The power of an electric UAV ranges from 100 W to 10,000 W. However, using a solar energy power generator results in climatic and topographical limitations. The combined heat and power (CHP) generators can generate heat and electricity simultaneously [2]. In high-altitude countries, the use of a heater or stove for heating a house is common. Qiu and Hayden [3] demonstrated the feasibility of TPV generation in boilers/furnaces for micro-CHP application in residential building. A Stirling engine can be connected to a micro-CHP for electricity generation with an output range of 10–1000 W. Although micro-CHPs can be used in daily life, engine operation is noisy because of the moving

☆ This paper is submitted for publication in ***Applied Energy***. Material in this manuscript has neither been published in nor submitted to a journal previously, nor will it be submitted to another journal during the ***Applied Energy*** review process.

* Corresponding author.
E-mail address: yueheng@mail.ncku.edu.tw (Y.-H. Li).

https://doi.org/10.1016/j.apenergy.2017.11.095
Received 2 October 2017; Received in revised form 16 November 2017; Accepted 24 November 2017

parts. Furthermore, the concept of one-person-portable power was proposed because of military demand to surpass logistical difficulties and the heavy weight of traditional power generators. Originally, JX Crystals Inc. designed a 230 W propane-firing recharger for the U.S. Army. In addition to military applications, one-person-portable power generation also had potential in civilian life because of the prevalence of electronic devices. The aforementioned applications all require power systems that have a small volume, light weight, uninterrupted power capability, adaptability to different environments, and high power density [4].

Microscale power generation systems are implemented in various forms, including the micro gas turbine [5], micro free-piston engine [6], micro thermoelectric device [7,8], and micro thermophotovoltaic (micro-TPV) system [9,10]. Although the current versions of these microsystems have low efficiency levels, these microsystems exhibit the potential to generate power on the order of a few watts within a volume of several cubic centimetres. Nevertheless, the concept of micro-TPV systems is straightforward: they directly convert thermal energy to electric energy through a photovoltaic (PV) array. The primary micro-TPV configuration comprises a heat source, an emitter, and a PV array [11,12]. Heat is absorbed by the emitter, which then emits radiation. The PV array converts the radiation into electricity. The heat source of TPV systems can be solar energy, nuclear energy, or chemical combustion. Compared with solar energy and nuclear energy, the combustion approach is not limited by climate, geographic conditions, and regulatory requirements. Combustion of hydrocarbon fuels is also regarded as a potential and feasible method to satisfy the power demands of present-day miniature devices thanks to the high energy density of hydrocarbon fuels (45 MJ/kg), which offer 10 times more power than sophisticated batteries do (0.5 MJ/kg) [13]. Additionally, micro-TPVs are compact, can be robotically assembled, and have neither moving components nor intricate structures that might produce friction and thus cause energy loss. Because micro-TPV systems offer high reliability and maintainability, this study centres on the development of micro-TPV power systems.

When combustor volume decreases, the ratio of surface area to volume increases, and the problems associated with heat loss appear. Heat loss through combustor walls tends to suppress ignition and leads to thermal quenching. When the temperature drops, the chemical reaction rate also declines due to thermal quenching, resulting in incomplete combustion. Therefore, very careful design is necessary in order to enhance stability and robustness of these systems and to improve combustion efficiency. Yang et al. [14] employed a backward-facing step in the microchannel. In this manner, flow recirculation was induced and anchored in the channel to improve the fuel–air mixture and overcome incomplete combustion [10]. Akhtar et al. [15] numerically discussed the flow and flame behavior in a micro TPV-reactor with different combustor geometries, and pointed out that the combustors with trapezoidal and triangular cross-section have better heat transfer capacity. Kim et al. [16] investigated the effect of Swiss-roll combustor configuration on the flame stabilization, and discussed the heat transfer behavior in a small Swiss-roll combustor. Ahn et al. [17] used a Swiss-roll burner to enhance the flame limit by using the exhaust gas to preheat the fresh fuel–air mixture. Zuo et al. [18] numerically investigated the thermal performance of counterflow and coflow double-channel combustor. Mujeebu et al. [19] adopted a porous medium burner to enhance the adiabatic flame temperature and effectively stabilise the flames in a microscale combustor. Additionally, Li et al. [20] designed a segment catalyst with cavities to successfully stabilise flames in a microscale combustor. The catalyst reduced activation energy and facilitated overcoming the thermal and radical quenching in the microchannel [21]. The cavities also provide a region of low velocity for stabilising the flame. According to the Stefan–Boltzmann law, photons produced at higher temperatures are more powerful, and so the radiation efficiency of the emitter can be enhanced. Therefore, increasing surface temperature of the emitter is necessary. Lu et al. [22] the effects of catalytic walls on the homogeneous combustion were investigated via varying catalyst segment layouts and sizes. Su et al. [23] pointed out that wall temperature of double-cavity combustor is more uniform and higher than that of single-cavity combustor. The radiation efficiency increases from 1.25% (single-cavity combustor) to 1.53% (double-cavity combustor). Yang et al. [24] investigated the effects of catalytic wall on combustion in the cylindrical micro-combustors, and found that the output electrical power of the system with platinum as catalyst is increased by 11–23.8% compared with that without platinum. Yang et al. [25] employed a silicon carbide (SiC) tube with heat recirculation to preheat the fresh mixture by the heat of exhaust gas; by means of heat recuperation, increased wall temperature and radiation of the emitter resulted. Lee and Kwon [26] designed a 1–10 W power-generating micro-TPV system and improved the performance of micro-TPV system with heat-recirculation concept. Park et al. [27] design a heat-recirculating micro-emitter fuelled with propane/air mixture. The output power and overall efficiency of the micro-TPV are 2.9% and 3.8 W. Because of the favourable management of heat exchange, the radiation and wall temperature of the emitter significantly improved. Alipoor and Saidi [28] discovered that the establishment of secondary flows and better preheating in the curved tube of micro-TPV reactor tends that the flammability limits to be at least four times in comparison with straight tubes.

The emitter's emitting material must be suitable for absorbing heat from the heat source and then transforming it into light. Several considerations must be taken into account [19]: First, optimal thermal stability and thermal shock resistance for tolerating the impact of high combustion temperatures, usually exceeding 1000 K. Second, a high thermal conductivity that leads to a uniform wall temperature over the emitter. Third, high emissivity to achieve a high radiative heat transfer rate. However, the most crucial requirement is that the radiative spectrum of the emitter matches the bandgap of the PV cells. Given the aforementioned considerations, ceramic is an appropriate candidate material for an emitter. Several studies have used oxide-based ceramics, such as Al_2O_3, ZrO_2, and MgO, as emitters for TPV systems; unfortunately, performance was insufficient because of poor thermal shock resistance and low emissivity. Silicon carbide (SiC) is employed as an emitter for non-oxide-based ceramics and boasts high temperature tolerance (approximately 1600 °C) and large emissivity similar to, for example, a black body. It is considered as a broadband emitter, for which the spectral range of radiation is 1000–3000 μm [29]. Most photons at near-infrared wavelengths cannot be transformed into electricity through PV cells, and unusable photons turn into heat and damage the PV cells. Alternatively, several studies have developed selective emitters that are based on transition metal oxides, such as ytterbia and erbia [30]. Owing to high-temperature stability and selective radiation [31], the wavelengths of ytterbia and erbia are approximately 900–1100 nm and 1300–1750 nm, respectively, at a surface temperature of 1373 K.

Currently, GaSb PV cells are regarded as the most plausible choice for TPV generators because of their low bandgap and maximal region of spectral conversion that can exceed 1800 nm. Compared with silicon-based PV cells (300–1100 nm), GaSb PV cells (250–1800 nm) transform a wider range of photons, from visible light to near-infrared light, into electricity. Most photons generated by the TPV systems congregate at the near-infrared portion of the spectrum. Consequently, using GaSb PV cells improves the quantum efficiency of the TPV system. Amano et al. [29] found that although Si cells generated only 0.11 W power, GaSb cells generated 0.25 W if flow velocity and equivalence ratio conditions were identical. Thus, GaSb PV cells are more appropriate for TPV systems than conventional silicon-based PV cells. Alternatively, Yang et al. [32] proposed the micro-combustor with SiC porous medium, and the corresponding overall efficiency is 0.92% when InGaAsSb PV cells are employed. Wu et al. [33] designed a radiant porous burner integrated with water-cooled GaSb PV cells, and the electrical output power

reaches to 9.5 W.

Depending on the process of miniaturisation, heat losses and incomplete conversion can be serious problems because of the high surface-to-volume ratios of small devices, which decrease overall efficiency. In a past study of micro-TPV systems, Yang et al. [34] employed an SiC tube as an emitter and hydrogen as fuel; the resulting system generated 0.92 W. Later, they not only used a SiC emitter but also a recirculator. With that setup, the system generated 1.36 W, and the corresponding overall efficiency increased to 0.86%. Su et al. [35] design a multiple-channel micro combustor for a micro-TPV system. Compared to single-channel combustor, the radiant energy and efficiency of multiple-channel combustor are both increasing. Qiu et al. [36] employed a selective radiator and natural gas. The system could generate output power of 8.3 W with a corresponding overall efficiency of 1.47%. Kwon et al. [27] designed a heat-recirculating emitter and used propane as fuel. The results show that the system generated 2.35 W with a corresponding overall efficiency of 2.12%. Park et al. [37] design a heat-recirculating micro-emitter fuelled with propane/air mixture. The output power and overall efficiency of the micro-TPV are 2.9% and 3.8 W.

To mitigate the heat loss and incomplete combustion occurring in these micro-devices, a platinum tube with a perforated ring serves double roles as the catalytic reactor and the emitter. The mechanisms of the backward-facing step and fuel deployment are addressed in the micro-TPV combustor. The fuel–air mixture is simultaneously delivered to the inner and outer chambers to prevent heat loss through the combustion chamber. Further, platinum is one of the noble metal catalysts that can reduce the activation energy and generate catalytically induced combustion, even in a microchannel. The catalytically induced combustion generates chemical exothermicity and then enhances the concentrations of radicals and intermediate species in the localised regime. These products all have considerable reactivity and facilitate the achievement of complete combustion. The presence of perforations on the platinum tube means that the heat and radicals generated between the adjacent catalyst surfaces help generate and sustain the gas phase reaction. The system stabilises the flame at the perforated holes and continuously supplies a stable heat source to heat the fuel–air mixture in the outer chamber. This implementation can extend the flame limit and effectively maintain the flame in the microchannel. Based on previous experience, this study attempts to enhance the overall efficiency of micro-TPV reactor by collecting radiations from emitter and combustion chamber. Fig. 1 shows a schematic of the micro-TPV combustor, and labels three individual types of radiation from different sources. The outer tube has two conditions. One is a transparent quartz tube that can simultaneously integrate the radiation of the flame and the platinum tube. The other is a semi-transparent quartz tube coated with metal-oxide particles. The metal oxide-deposited layer can be incandescent while absorbing thermal energy from flames. However, the proper fuel deployment and fluid design for the micro-TPV reactor are strongly associated with combustion stability and radiant intensity of the micro-TPV reactor. Therefore, this study discusses the system performance of the micro-TPV reactor with regard to combustion, thermal radiation, and electrical output.

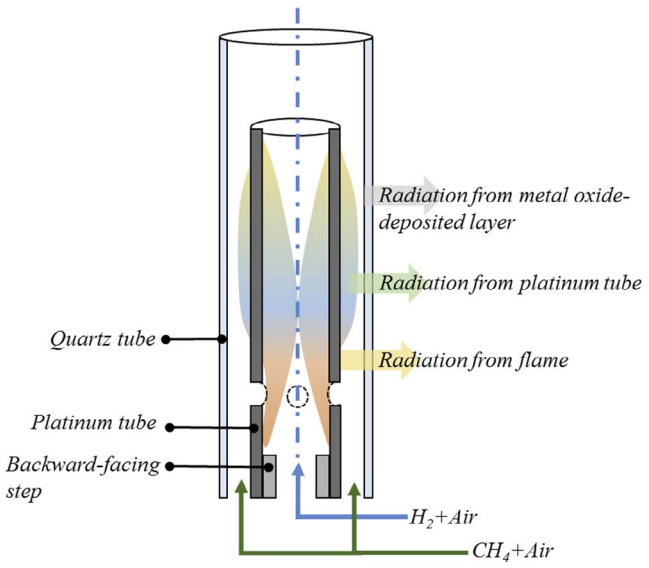

Fig. 1. Schematic of the proposed micro-TPV combustor.

2. Flame stabilization mechanism of micro-TPV reactor

The flame stabilization mechanism of the micro-TPV combustor originates from the similar concepts of the microchannel with catalyst segmentation and cavity and the heat recirculation of a Swiss-roll combustor. The configuration of the micro-TPV combustor consists of two platinum tubes of identical width measuring 5.3 mm (inner diameter) × 6 mm (outer diameter). A 4.5-mm-long tube is placed in the upstream and a 24.5-mm-long tube is placed in tandem with a gap of 1 mm. The platinum tubes are coaxially placed in a quartz tube, of which the dimensions are 8 mm (inner diameter) × 10 mm (outer diameter) × 50 mm (length). This coaxial reactor constitutes the central (inner) chamber and the annular (outer) chamber. Sustaining maximal incandescent illumination over the platinum tubes with minimal fuel consumption is the ultimate purpose. Furthermore, H_2 is prone to inducing heterogeneous reactions over the platinum surface because of highly sticking coefficient. Consequently, an H_2–air mixture is delivered to the inner chamber of the reactor to generate a heat source at the reactor wall. By contrast, CH_4 has a high volumetric energy density (37.8 kJ/L) compared with hydrogen (10.1 kJ/L), and thus inducing catalytically stabilised CH_4–air flame in the outer chamber capitalised on improving the incandescence of the micro-TPV combustor.

To demonstrate and verify that the aforementioned concept is feasible in a micro-TPV combustor, a numerical simulation was performed with a commercial CFD-ACE+. Chemical reaction mechanisms were simulated in the gas phase as well as on the catalyst surface. In this study, the GRI-3.0 mechanism was used for CH_4–air/H_2–air combustion, and it comprised 53 species and 325 reaction steps. The surface reaction mechanism was compiled primarily from that proposed by Deutschmann et al. [38]. The reaction mechanisms have been used in previous studies [20,39,40], and the comparisons with experimental results were satisfactory [41]. The equivalence ratio of the H_2–air mixture was 0.5 for the inner tube and that of the CH_4–air mixture was 0.6 for the outer tube. The inlet temperature was 300 K and a uniform velocity profile was specified at the inlet at a fixed value of 10 m/s. At the exit, pressure was specified with a constant ambient pressure of 101 kPa, and an extrapolation scheme was used for species and temperature.

Generally, sustaining catalytic micro combustion of methane over platinum is not as straightforward as over hydrogen. Methane is inherently weak in hybrid heterogeneous and homogeneous coupling. It requires a long catalyst length with a high surface temperature for complete conversion over platinum [42] or addition of hydrogen in a methane–air mixture for sustaining the hybrid hetero- or homogeneous combustion [43]. In a previous study, numerical results led to the discovery of the flame-stabilising mechanism of the microsegment platinum tubular reactor with a gap. The interaction of heterogeneous and homogeneous H_2 reactions in the vicinity of the gap was discussed in terms of the effect of reactor configuration and fuel concentration. However, the flame radiation of hydrogen was too weak, and so hydrogen was substituted for methane as the fuel in the outer chamber to induce the methane gas phase reaction. To examine the flame stabilization mechanism in microreactors, two different platinum reactors, namely a plain platinum tube and two platinum tube segments with a gap, were employed to investigate the effects of the reactor

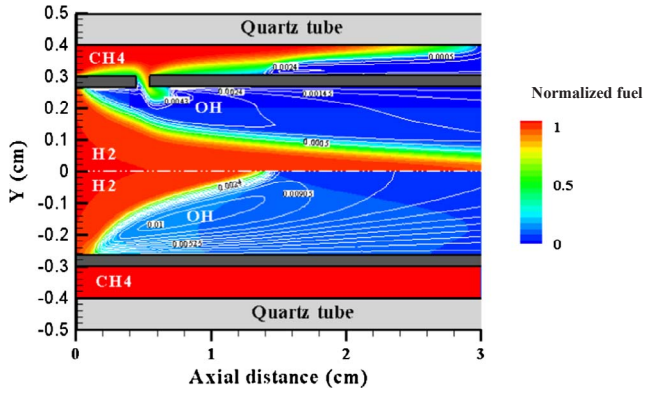

Fig. 2. Local distributions of normalized fuel mass fractions with overlaid OH radical concentration level lines for two reactor configurations in the fixed velocity of 10 m/s.

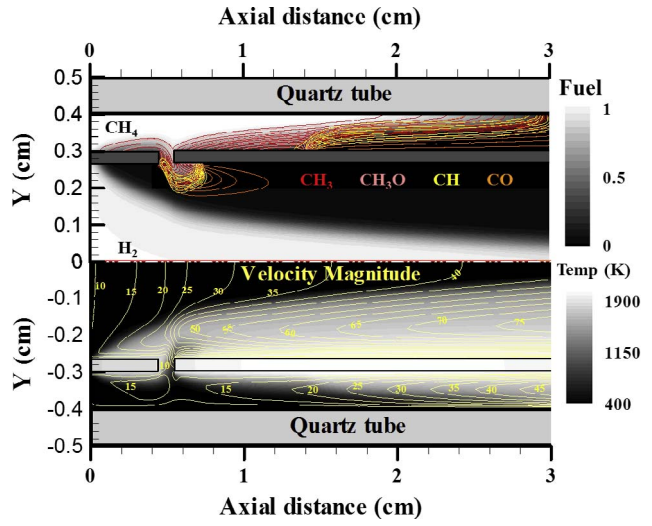

Fig. 3. (a) The local distribution of normalized fuel mass fractions overlaid with radical concentration level lines, (b) temperature distribution with overlaid velocity magnitude level lines for ER_{in} = 0.5 and ER_{out} = 0.6 at the fixed velocity of 10 m/s in the first 3 cm distance of the micro-TPV reactor.

configuration and fuel/air deployment on the performance of the micro-TPV reactor. Fig. 2 illustrates the local distributions of normalized fuel mass fractions overlaid with OH radical concentration level lines for the two reactor configurations at a fixed velocity of 10 m/s. For the case of the plain platinum reactor, a catalytically induced homogeneous reaction of hydrogen was engendered and sustained in the inner chamber when the equivalence ratio of the H_2–air mixture rose to a stoichiometric condition (Fig. 2, lower panel), but the methane in the outer chamber had no significant reaction; this was assumed to be because the heat source on the catalytic surface was not sufficient to induce the chemical reaction of methane in the outer chamber. For the segmented platinum reactor, the catalytic combustion of methane was successfully sustained on the inner surface of the second platinum tube segment, with equivalence ratio of the H_2–air mixture being 0.5. Although a certain portion of methane flowed into the inner chamber through the gap, most methane was completely consumed within a 3-cm distance. Fig. 3 illustrates the local distribution of normalized fuel mass fractions overlaid with radical concentration level lines in the upper panel, and temperature distribution overlaid with velocity magnitude in the lower panel. Given the distribution of velocity magnitude and fuel concentration, the gap between two segment tubes provided a relatively low velocity zone to decelerate the flow in localised spaces and doubled as a channel to trade and collect the fuel and radicals from the two sides. The distribution of OH contour indicates catalytically stabilised thermal gas phase reaction was sustained on the inner and outer surfaces. The catalytic combustion of methane was successfully sustained on the outer surface of the second segment of platinum tube. Although a certain portion of the methane flowed into the inner chamber through the gap, most methane was completely consumed within a 3-cm distance. In the upstream segment platinum tube, H_2 was initially consumed over the inner catalyst surface, providing a heat source to promote the chemical reaction of methane over the outer catalyst surface. The surface reaction–induced thermal expansion of the mixture in the outer chamber propelled the mixture towards the inner chamber through the gap because the space in the outer chamber was narrow compared with that in the inner chamber. Therefore, CH_4–air mixture flowed towards the inner chamber through the gap, and CH_4 mass fraction evidently increased near the gap. Furthermore, H_2 branched-chain reactions in the inner chamber yielded plentiful radicals, such as O, H, and OH. Those radicals promote progressive dehydrogenation of CH_4 to CH_3 and CH_3O, then to CH_2O, HCO, and finally oxidation of CO to CO_2. In the upper panel of Fig. 3, the evolution of methane consumption is obvious indicated in the channels. The CH_3 and CO mass fractions in the gap testified to the methane consumption, and the yield of chemical radicals was advantageous for accelerating methane consumption and inducing the catalytic combustion of methane on the downstream segment of the platinum tube.

Fig. 4 shows the fuel and radical mass fractions along the axial direction close to the inner and outer surfaces of the segmented platinum reactor over the first 2-cm distance. In the upstream platinum tube segment, H_2 was initially consumed on the inner catalyst surface, providing a heat source to promote the heterogeneous reaction of methane on the outer catalyst surface. The distribution of the methane mass fraction in the gap evidently increased in the inner and outer chambers because of the methane diffusion driven by the tangential flow velocity. In addition, the incremental CH_3 and CO mass fractions in the gap revealed the inception of methane dissociation and further engendered the generation of abundant chemical radicals such as H and OH. The chemical radical yield was advantageous to accelerate the methane dissociation and induce the catalytic combustion of methane on the downstream platinum tube segment. This was proven by the increase in the CH_3 and OH mass fractions, followed by an abrupt drop in the CH_4 mass fraction along the outer surface of the downstream platinum tube segment. Fig. 5 illustrates the ratios of the surface mass fraction (Y_s) to the mean bulk mass fraction (Y_b) along the inner and outer surfaces of the platinum tubes. In general, the heterogeneous reaction can be

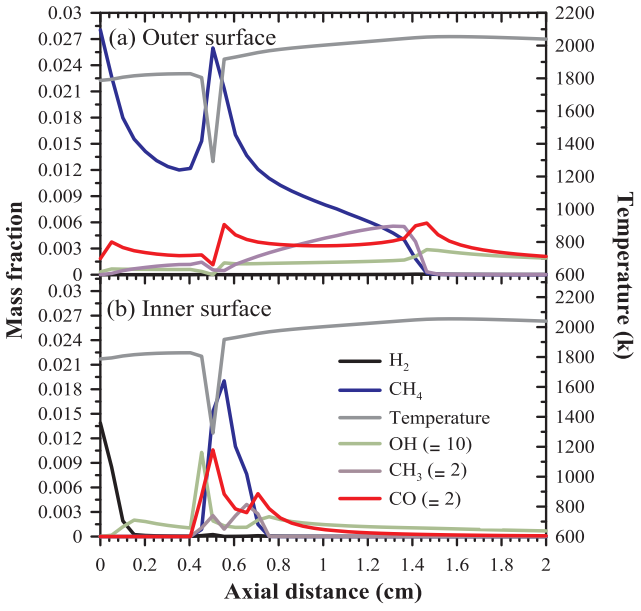

Fig. 4. The fuel and radical mass fractions along the axial direction close to the (a) inner and (b) outer surfaces of the segmented platinum reactor in first 2 cm distance.

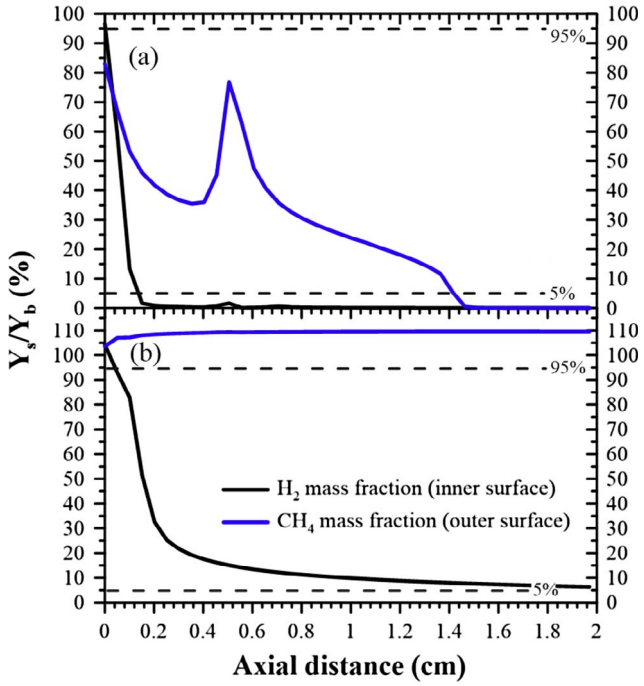

Fig. 5. Fuel mass fraction along the inner and outer surfaces of (a) segmented platinum and (b) plain platinum reactor.

considered as a kinetically controlled reaction, for which the surface concentration is greater than 95% of the bulk concentration, and as a mass transfer controlled reaction, for which the surface concentration is less than 5% of the bulk. For the case of the plain platinum reactor, this study determined almost no chemical reaction of methane, but hydrogen was significantly consumed along the inner catalyst surface. For the case of the segmented platinum reactor, methane was completely consumed by the successful ignition of the gas phase reaction of methane in the downstream segment, and the heterogeneous reaction of hydrogen can be considered to be a mass transfer controlled.

3. Experimental apparatus

3.1. Dimensions of micro-TPV reactor

The micro-TPV reactor comprised a platinum tube with the dimensions 5.3 mm (ID) × 6 mm (OD) × 30 mm (L), whereas the quartz tube was 8 mm (ID) × 10 mm (OD) × 160 mm (L). The quartz tube was installed to surround the platinum tube. The platinum tube included eight perforations (1 mm in diameter) equidistantly placed around the tube at a distance of 5 mm from the bottom of the tube. The platinum tube was mounted on the flange of a stainless steel tube, which measured 4 mm (ID) × 5.3 mm (OD), and featured a backward-facing step (length: 5 mm) in the connection section. A metal oxide–deposited quartz tube functioned as an emitter; it measured 8 mm (ID) × 10 mm (OD) × 160 mm (L). Fig. 6 shows a schematic and photograph of (a) the micro-TPV reactor and (b) the metal oxide–deposited quartz emitter.

3.2. Measurement system

The wall temperature of the micro-TPV reactor was monitored by using an infrared thermometer (Raytek, CA, USA, model RAYMA2SCCFL). A small pump with an elongated needle extracted the flue gas in the downstream of the quartz tube into a 1L sampling bag. A Gas Chromatography (GC) was employed for analysing the composition of the flue gas. An integrating sphere connected with a spectrometer was employed to measure the irradiation of the emitter. The integrating sphere (diameter: 15 cm) had magnesium oxide (MgO) deposited on its

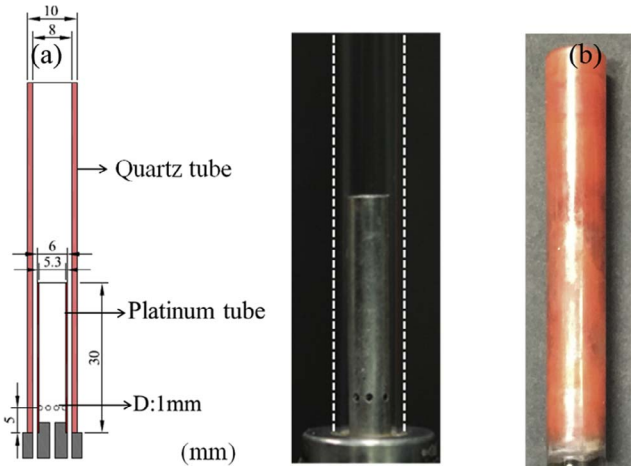

Fig. 6. (a) Schematic and photograph of the micro-TPV reactor, (b) photograph of a metal oxide–deposited quartz emitter.

inner surface. Integrating spheres are employed for a variety of optical, photometric, or radiometric measurements, and used for measuring the total light radiated in all directions from a light source. Accordingly, they can be used to measure the diffuse reflectance of surfaces, providing averages over all angles of illumination and observation. The spectral wavelength of the spectrometer (Ocean Optics Inc., FL, USA) ranged from 200 nm to 1050 nm. For measurement, the emitter was placed in the centre of the integrating sphere so that the emitted radiation scattered and distributed uniformly onto its surface. The spectrometer was connected to the integrating sphere, allowing the radiation flux to be obtained. By multiplying by the surface area of the emitter, total irradiation could be determined. Fig. 7 presents a photograph of the measurement system.

A monochromator (Spectral Products Company, CT, USA, model DK240) with IR photoresistor (Spectral Products Company, model AD131-USB) was used to measure the spectral distribution of the emitter. The scanning spectrum spanned 400–1500 nm. The radiation was collected and introduced to the slit of the monochromator by a convex lens set, after which the IR photoresistor absorbed and converted the radiation into the current single. In this manner, the spectrum distribution of the radiation from the emitter could be detected.

3.3. Thermophotovoltaic cell array

According to the measured spectrum distribution of emitting radiation, the maximal spectrum intensity of emitting radiation is congregated within 1100–1400 nm, while the absorption spectrum of commercial GaSb cell (JX Crystals, WA, USA) spans from 400 to 1800 nm. Consequently, it is appropriate to utilize GaSb cells for energy conversion instead of silicon-based PV cells. In this study, the combustor was surrounded by a PV cell array, which was connected with an electric load device (Prodigit, New Taipei City, Taiwan, 331D). The selected PV cell array comprised 2 × 12 GaSb single cells, as shown in Fig. 8. The specifications of the PV cell array are listed as follows:

Open circuit voltage (V_{oc}): 23.023 V;
Short-circuit current density (I_{sc}): 2.9875 A/cm^2;
Fill factor (FF): 0.733;
Maximum open circuit voltage: 17.769 V;
Maximum short-circuit current density: 2.5754 A/cm^2;
Maximum power density: 45.763 W/cm^2.

To measure the power of the micro-TPV system, the electric load was engaged to assess power performance. This electric load was controlled by a computer by using GPIB and RS232. In addition, four

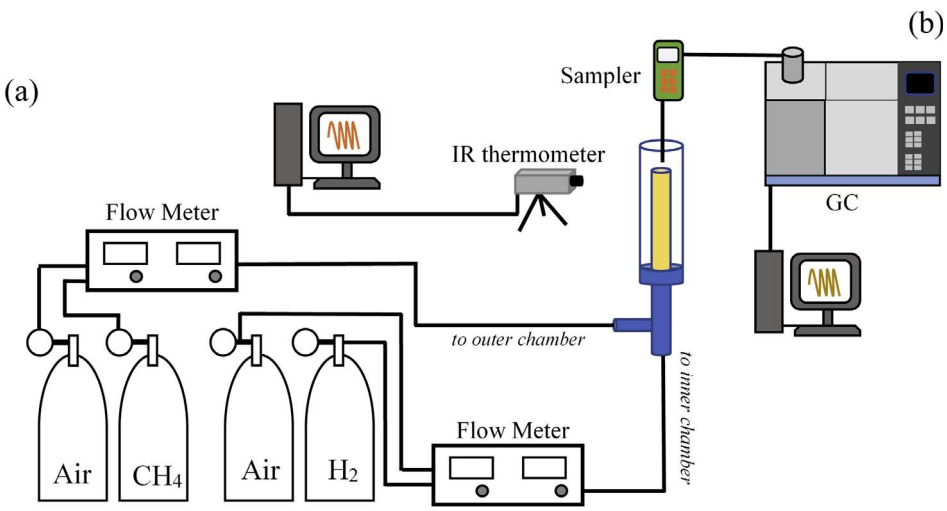

Fig. 7. (a) The schematic of experimental apparatus and measurement system, (b) photograph of the integrating sphere assembled with the spectrometer.

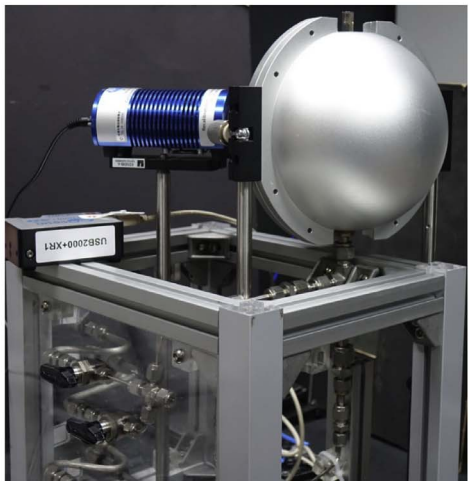

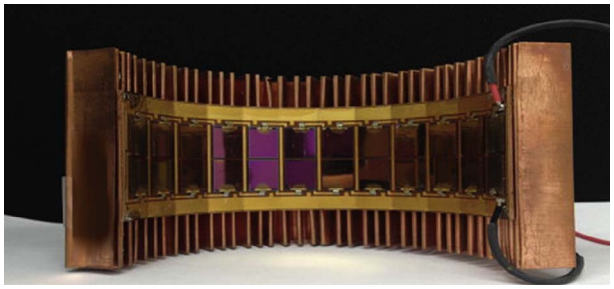

Fig. 8. Photograph of the PV cell array, fabricated by JX Crystals.

modes detected five components, namely constant current, constant resistance, constant voltage, constant power, and short circuit, which provided information regarding the corresponding values such as voltage, current, and power. In this study, the I-V curve could be determined by adjusting various resistances. The selective resistance spans from 0.5 to 101.35 Ω, and the total amount of selective resistance is 90.

4. Results and discussion

4.1. Combustion characteristics

Although methane and hydrogen are considered highly energy-dense fuels, the chemical reactivity level and sticking coefficient of methane on platinum are much lower than those for hydrogen, so methane does not ignite easily on platinum. Methane requires a higher surface temperature and larger catalytic area of the platinum tube to achieve a complete conversion. Therefore, heat release of the hydrogen–air mixture in the inner chamber is associated with the successful induction of methane catalytic combustion in the outer chamber. Fig. 9 illustrates the combustion of the micro-TPV reactor under different inner equivalence ratios of the hydrogen–air mixture with the constant outer equivalence ratios of methane–air mixture (ER_{out} = 0.7). In the case of ER_{in} equal to 0.5, the luminosity of the microreactor is dim red[1] with a weak irradiance of 1356 W/m^2. Heat release of hydrogen–air reaction inside the chamber appears insufficient for inducing the methane catalytic combustion in the outer chamber. When ER_{in} rises to 0.6, the luminosity of the microreactor apparently increases and is orange-coloured. Corresponding irradiance reaches 6858 W/m^2. The chemical exothermicity generated by H_2–air reaction in the inner chamber seems to partially facilitate the chemical reaction of methane in the outer chamber. However, when ER_{in} rises to 0.7, the chemical exothermicity of H_2–air mixture surpasses the thermal energy required for sustaining methane catalytic combustion in the outer chamber. The luminous colour turns to bright yellow, and the luminosity distribution becomes uniform. The measured irradiance of the micro-TPV rises to 24,718 W/m^2. When the ER_{in} increases to 0.8, the luminous intensity of

[1] For interpretation of color in 'Fig. 9', the reader is referred to the web version of this article.

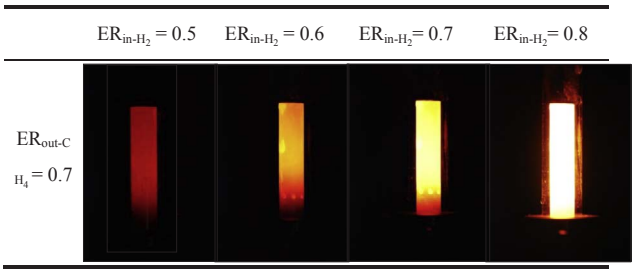

Fig. 9. Combustion of the micro-TPV reactor under different ER_{out} of the CH_4–air mixture with constant ER_{in} of 0.6 and 0.7 for the H_2–air mixture.

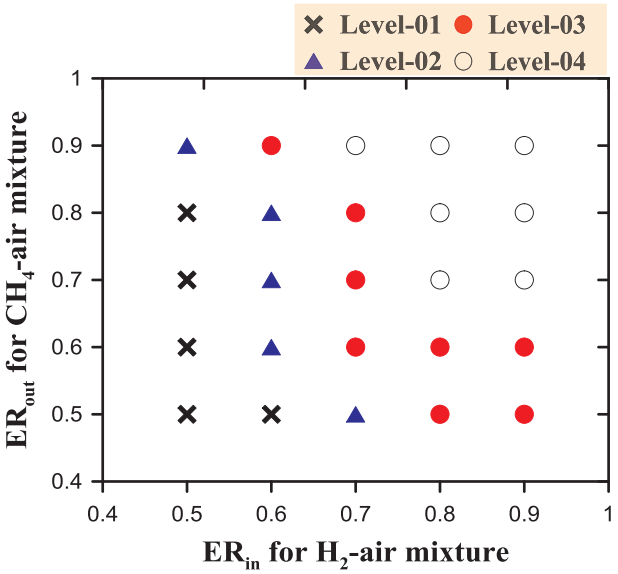

Fig. 10. Operating range of luminous emissions of the micro-TPV reactor under different ER_{out} levels of the CH_4–air mixture and different ER_{in} levels of H_2–air mixture.

the microreactor increases to 52,200 W/m^2, and the luminous colour becomes bright white. According to irradiance, the luminosity of the micro-TPV can be classified into four levels: Level 1 (less than 2500 W/m^2), Level 2 (greater than 2500 and less than 15,000 W/m^2), Level 3 (greater than 15,000 and less than 40,000 W/m^2), and Level 4 (greater than 40,000 W/m^2). Technically, the luminosities of Levels 2, 3, and 4 are appropriate to convert into electricity using the TPV cells, but Level 2 has incomplete combustion of methane–air mixture and low luminosity, which is unfavourable to energy conversion. In addition, Level 4 has an extremely high wall temperature and it may deteriorate the structural integrity of the platinum tube. Fig. 10 presents the operating range of the luminous emissions of the micro-TPV reactor under different ER_{out} values of the CH_4–air mixture and ER_{in} of H_2–air mixture. The minimal ER_{in} of hydrogen–air mixture in the inner chamber is 0.6 to guarantee the inception of methane catalytic combustion in the outer chamber. In addition, when the ER_{in} of hydrogen–air mixture is fixed, the luminosity of the micro-TPV apparently increases with an increase in ER_{out} of CH_4–air mixture.

To examine the combustion efficiency of the micro-TPV reactor, three conditions were selected for further estimation, ER_{out,CH_4} = 0.5, 0.7, and 0.9 with a consistent ER_{in,H_2} = 0.7 and flow velocity of 6 m/s. Fig. 11 shows the combustion of the micro-TPV reactor in three conditions. The corresponding surface temperature distribution of the three conditions is presented in Fig. 12. The averaged surface temperatures gauged by the infrared thermometer were greater than 1300 K. Therefore, it can be inferred that the methane catalytic combustion can be sustained in the outer chamber in these three conditions. To examine the consequences of catalytic combustion, the remaining CH_4 and H_2 concentration in flue gas was detected through the GC–TCD, and then

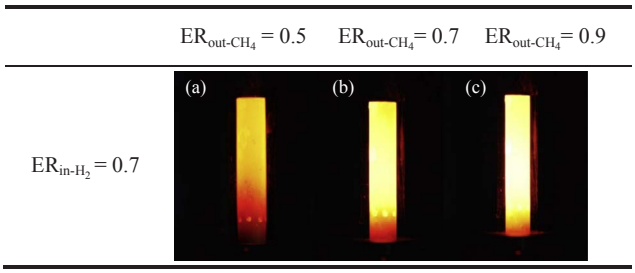

Fig. 11. Combustion of the micro-TPV reactor under different ER_{out} of the CH_4–air mixture equal to (a) 0.5, (b) 0.7, and (c) 0.9 with constant ER_{in} of 0.7 for H_2–air mixture.

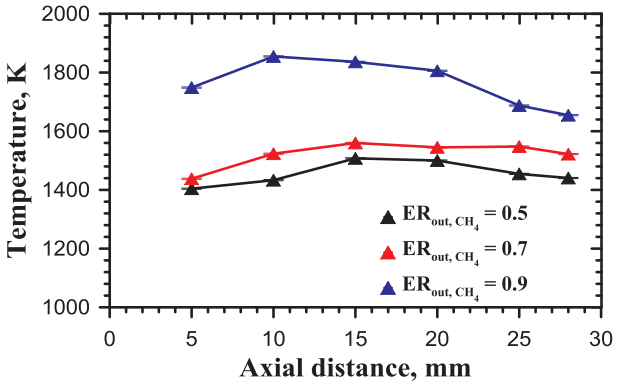

Fig. 12. Surface temperature distribution along the micro-TPV.

the fuel conversion rate was determined. The results indicate that hydrogen conversion rates for the three conditions are 100% because no H_2 remained in the flue gas. Nonetheless, the methane conversion rates were 84.16% for the case of ER_{out,CH_4} = 0.5, 88.62% for the case of ER_{out,CH_4} = 0.7, and 100% for the case of ER_{out,CH_4} = 0.9, which testifies to the existence of methane catalytic combustion. The previous numerical results showed that CH_4 may flow to the inner chamber through the perforated holes and initiate the catalytically induced gas phase reaction with the assistance of outward-diffused radicals from hydrogen–air reaction. However, the increasing methane concentration in the outer chamber can enrich inflowed methane in the inner chamber and enhance the exothermicity of the catalytically stabilised gas phase reaction in the inner chamber. The enhanced surface temperature in turn accelerates the methane consumption in the outer chamber. Eventually, the enhanced combustion strength contributes to the increase in the irradiance of the TPV combustor.

The catalyst may be subject to deactivate its catalytic activity and selectivity. Argyle and Bartholomew [44] categorised the mechanisms of solid catalyst deactivation into six intrinsic mechanisms of catalyst decay: (1) poisoning, (2) fouling, (3) thermal degradation, (4) vapor compound formation, (5) vapor-solid and solid-solid reaction, (6) attrition and crushing. The tubular TPV-reactor is made of metal platinum, not coated platinum powder on the porous substrate, such as that used in a honeycomb catalyst. There are no issues associated with points 4 and 5. Furthermore, carbon monoxide is not delivered to the chamber as fuel in the TPV-reactor, so there are no risks of poisoning. High temperatures hinder carbon formation. In addition, Fig. 12 shows that the surface temperatures of the platinum reactor are below 1900 K, less than the melting point temperature of platinum (approximate 2041 K), so that the high surface temperatures do not jeopardize the integrity of platinum reactor. Regarding to repetitious ignition, it is prone to reignite the micro-TPV reactor by delivering hydrogen/air mixture into the inner chamber. Consequently, the micro-TPV reactor is compatible with hydrogen at high temperature conditions.

4.2. Thermal radiance

In general, the micro-TPV reactor converts the enthalpy of combustion released in the gas phase to radiant energy. This involves two heat transfer processes. One is convective heat transfer between gas and burner surface; the other is conversion of thermal energy into radiation. Radiation output depends on the emitter surface temperature and its radiative properties. In this study, the radiant efficiency was engaged to assess conversion efficiency. The radiation efficiency is the ratio of net radiant power output to actual fuel energy input. The radiant power output refers to the amount of radiation emitted from the micro-TPV reactor and from flame luminosity. However, the radiant power output from a micro-TPV reactor is usually measured using a radiometer. Perturbations of combustion and fluid dynamics may lead to non-uniformity of the TPV radiation, and a radiometer can accurately measure dynamic flame luminosity in the outer chamber. Therefore, to mitigate the uncertainty of irradiation measurement, the micro-TPV reactor was, at first, placed in the centre of the integrating sphere. As the radiation of the combustor scattered uniformly in the integrating sphere, an optical fibre collected the radiation in the integrating sphere and sent the signal to a spectral meter to measure the irradiance. Accordingly, the radiant power output can be calculated by multiplying measured irradiance and surface area of the reactor. Actual fuel conversion was considered for actual fuel energy input. Table 1 presents the results of radiant intensity of the micro-TPV reactor under the different equivalence ratios of methane–air mixture with the fixed velocity of 6 m/s. Apparently, the irradiance of the TPV reactor increased with increasing methane injection. Maximum irradiance reached 51,100 W/m^2 with a corresponding radiant efficiency of 6.50% when methane was ER_{out} = 0.9 and hydrogen was ER_{in} = 0.7. This has more than fourfold greater radiant efficiency compared with the case of ER_{in,H_2} = 0.7 and ER_{out,CH_4} = 0.5. Low radiant efficiency is because only partial chemical exothermicity of input fuel is exerted on the micro-TPV reactor, and major thermal release remains in the flue gas and is dumped into the ambient atmosphere. Therefore, how to extract more energy from flames is a priority for improving the radiant efficiency of this micro-TPV reactor.

On the basis of the quantum efficiency of GaSb PV cells, the optimal wavelength for energy conversion is in the range 500–1800 nm. To maximise the energy conversion of the TPV cell, the spectrum distribution of the micro-TPV reactor was detected using a monochromator with an IR photoresistor. The results show that most of the radiation spectrum congregates in the range 600–1500 nm (Fig. 13). Depending on the increasing ER_{out,CH_4}, the spectral distribution shifts to a shorter wavelength because of the increasing irradiance. Moreover, the methane hydrogen–air combustion conforms to the range that can be absorbed by the GaSb PV cells, which and verifies that the methane hydrogen–air combustion is suitable for use with a GsSb PV cells array.

In our previous study, a metal oxide layer–deposited quartz tube was developed, which used an emitter. The principal characteristic of this quartz emitter is semitransparency, and it can emit radiation and simultaneously allow flame luminosity to penetrate outwardly.

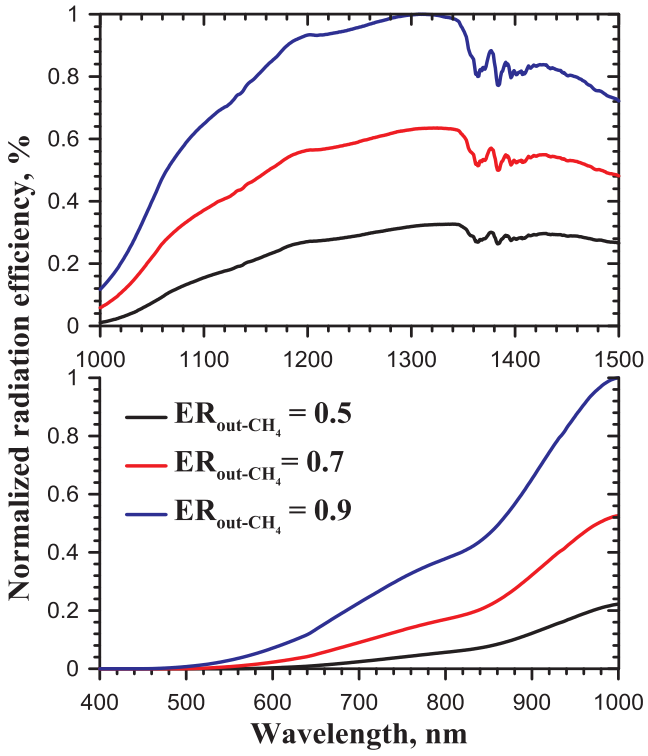

Fig. 13. Spectrum distribution for H_2–CH_4–air condition (400–1500 nm).

However, because methane catalytic combustion is sustained in the outer chamber, chemical energy can be further converted to radiant energy by replacing transparent quartz with metal oxide layer–deposited quartz. Ideally, collecting radiation from the quartz emitter, platinum tube, and flames simultaneously should be possible. Table 2 shows that the irradiance of the metal oxide–deposited quartz tube with the platinum emitter was on average lower than that of the transparent quartz tube with the platinum emitter. Under identical fuel conditions, namely ER_{out,CH_4} = 0.9 and ER_{in,H_2} = 0.7, the irradiance of the transparent quartz emitter with the platinum reactor was sixfold more than that of the metal oxide–deposited quartz emitter with the platinum reactor. The result of radiant measurement did not meet expectations. The quartz emitter somehow absorbed or blocked some specific radiation emitted from the inside of the TPV reactor. For identifying this situation, samples of the metal oxide–deposited quartz and transparent quartz were tested in an integrating sphere, and the absorption spectrum of the specimen was determined through a UV/visible/NIR spectrophotometer with a range from 200 nm to 1800 nm. The results indicated that the absorption spectrum of the metal oxide–deposited quartz specimen ranged from 200 nm to 1800 nm, and the maximal absorption spectrum congregated in the visible wavelengths (Fig. 14).

Table 1
Experimental results of radiant intensity for the micro-TPV reactor with a transparent quartz tube or a metal-oxide deposited quartz emitter.

Fuel/air mixture	CH_4 conversion rate, %	Irradiance, W/m^2	Radiant efficiency, %
ER_{in,H_2} = 0.7, ER_{out,CH_4} = 0.5	84.2	7791	1.38
ER_{in,H_2} = 0.7, ER_{out,CH_4} = 0.7	88.6	24,718	3.75
ER_{in,H_2} = 0.7, ER_{out,CH_4} = 0.9	100	51,100	6.50

Table 2
Experimental results of radiant intensity for the micro-TPV reactor.

Fuel/air mixture	Irradiance, W/m^2	
	Platinum tube + metal-oxide deposited quartz emitter	Platinum tube + transparent quartz tube
ER_{in,H_2} = 0.7, ER_{out,CH_4} = 0.5	< 10	7791
ER_{in,H_2} = 0.7, ER_{out,CH_4} = 0.7	2277	24,718
ER_{in,H_2} = 0.7, ER_{out,CH_4} = 0.9	8334	51,100

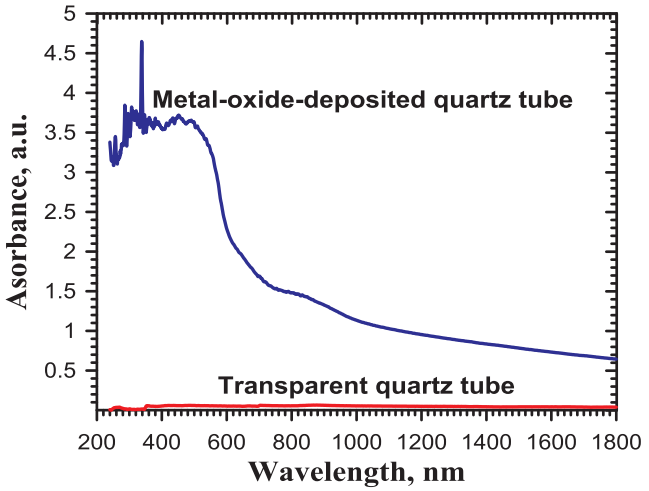

Fig. 14. Absorption spectrum for transparent quartz and metal oxide–deposited quartz specimens.

By contrast, the quartz specimen was approximately transparent to incident light of which the wavelength was larger than 4000 nm; therefore, this implies that the metal oxide–deposited quartz absorbed most of the radiation from the emitter, which led to lower irradiance.

4.3. Power performance

To evaluate the benefit of improving the micro-TPV reactor, GaSb PV cells were employed to collect luminosity and convert it into electricity. Effective power efficiency (η_r) is defined as the ratio of output power to radiation power, and overall efficiency (η_t) is defined as the ratio of output power to heat release rate of the fuels. The power output under the condition of $ER_{in\text{-}H_2} = 0.7$ and $ER_{out\text{-}CH_4} = 0.9$ at a velocity of 6 m/s was measured to be 0.94 W with an η_r of 3.24% and η_t of 0.11% (Table 3). However, a portion of the incandescence leaked to the environment through the top opening of the PV cell array. To improve the overall efficiency of the micro-TPV power system, a mirror with a diameter of 10 cm (OD) × 3 cm (ID) was installed on top of the PV cell array (Fig. 15a). The resulting output power with the mirror could then reach 1.18 W, and the corresponding η_r and η_t increased to 4.07% and 0.14%, respectively. To enhance the overall efficiency of the micro-TPV system, however, a recirculating cap was used to redirect the hot flue gas to heat the quartz tube and reduce heat loss (Fig. 15b). Under $ER_{in\text{-}H_2} = 0.7$ and $ER_{out\text{-}CH_4} = 0.9$; the output power of the micro-TPV reactor augmented with a mirror and a recirculating cap was 2.21 W with η_r and η_t of 6.32% and 0.26%, respectively.

According to aforementioned challenges of the miniaturization process, an appropriate flame stabilization mechanism is crucial in design of the combustion-driven TPV power system. Undoubtedly, providing stable burning in the small confinement and uniform distribution of temperature along the wall can achieve good performance of micro-TPV system in terms of thermal irradiance and power output. Compared with the present work, some promising micro-TPV systems are enumerated in Table 4. A backward-facing step is a straightforward mechanism to stabilise flames in small confinement. Flame anchoring

Table 3
Overall efficiency levels for various combustion configurations.

Fuel/air mixture	Power, W	η_r, %	η_t, %
$ER_{in,H_2} = 0.7$, $ER_{out,CH_4} = 0.9$	0.94	3.24	0.11
$ER_{in,H_2} = 0.7$, $ER_{out,CH_4} = 0.9$, with a mirror	1.18	4.07	0.14
$ER_{in,H_2} = 0.7$, $ER_{out,CH_4} = 0.9$, with a mirror and recirculating cap	2.21	6.32	0.26

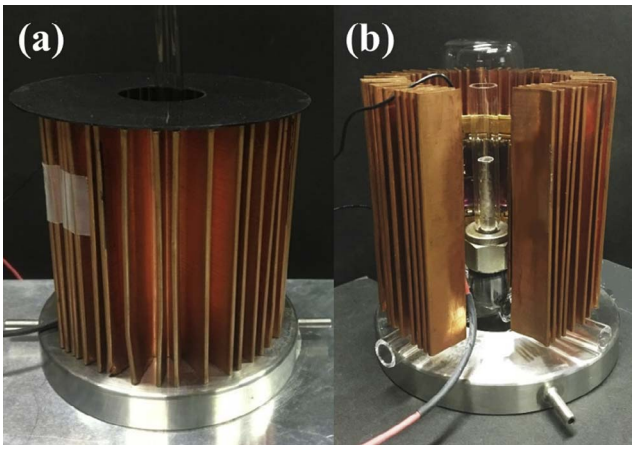

Fig. 15. Photograph of the PV cell array augmented with (a) a mirror and (b) a recirculating cap.

position is sensitive to flow intensity and recirculation pattern, leading to uneven incandescence on the emitter. Accordingly, applying a recuperator with the micro combustor is a plausible solution to cope with the incandescent non-uniformity on micro emitter. Yang et al. [14] designed a micro cylindrical combustor with a quartz recuperator, which is employed to recycle the waste heat of the hot exhaust gas to reheat the exit end of the micro combustor. Therefore, a higher and uniform wall temperature can be obtained, and the power output is 1.36 W in the condition of stoichiometric hydrogen/air mixture. Similarly, Park et al. [27] proposed a micro-emitter with an annular-type shield. Applying a heat-recirculation concept and an expanded exhaust outlet can facilitate ignition and provide stable burning in the small confinement. In addition, a porous medium burner can enhance the adiabatic flame temperature and stabilise the flames in a microscale combustor. For instant, Yang et al. [26] employed SiC porous medium foam in a micro modular combustor. The porous medium can enhance heat transfer between the hot gas and the wall. Packing the microcombustor with SiC porous medium is an effective method to increase the wall temperature, subsequently increasing the radiation energy of the micro-TPV system. Assembling the combustor with GaSb and InGaAsSb PV cells can produce 13.1 W and 6.1 W, respectively. However, owing to the larger thermal capacity of ceramic porous inert medium, it takes time to reach stable combustion. Packing the porous medium in the micro combustor is not a straightforward task. In the present work, a tubular platinum tube with a ring of perforated holes uses as a micro combustor and doubles a TPV-emitter simultaneously. Metallic platinum tube is prone to reach a uniform incandescent surface because of catalyst surface and high thermal conductivity. In addition, hydrogen/air mixture delivered to the inner chamber is used to sustain catalytic combustion inside the chamber and induce the chemical reaction of methane/air mixture outside the chamber. Power output of the present work can reach to 2.21 W in the condition of $ER_{in,H_2} = 0.7$ and $ER_{out,CH_4} = 0.9$. The corresponding overall efficiency is not remarkable by far. The main reason is that major energy still remains in the flue gas in spite of complete fuel conversion. However, assembling a heat exchange unit of water heating system with the TPV-reactor could extract thermal energy from the flue gas, and in the meantime, it fulfils the concept of the combined heat and power system.

5. Conclusion

To enhance the radiant intensity of the micro-TPV reactor, a platinum tube with a ring of perforated holes was employed with specific fuel deployment and discussed in terms of combustion behavior and radiant intensity. A hydrogen–air mixture was introduced to the inner chamber of the micro-TPV reactor to provide a thermal source, and a

Table 4
The comparison of present micro-TPV power system.

	Descript	System performance
Li et al., Present work	Using a tubular platinum tube with a ring of perforated holes as a micro combustor and a TPV-emitter in the same time. The purpose is to integrate radiation of flame luminosity and emitter incandescence. The fuel concentration of H_2/air mixture in inner chamber is associated with the induction of CH_4/air chemical reaction in outer chamber	Fuel type: H_2 (ER = 0.7)/CH_4 (ER = 0.9) PV cells: GaSb Output power: 2.21 W
Yang et al. [14]	A micro cylindrical combustor with recuperator. The inner combustor is made of SiC, and a backward facing step is designed to prevent the back flow of the flame. A cylindrical quartz recuperator is employed to recycle the waste heat of the hot exhaust gas to reheat the exit end of the micro combustor. Therefore, a higher and uniform wall temperature can be obtained	Fuel type: H_2 (ER = 1.0) PV cells: GaSb Output power: 1.36 W
Park et al. [27]	The micro-emitter with an annular-type shield is to apply a heat-recirculation concept and an expanded exhaust outlet that facilitates ignition, which provides stable burning in the small confinement and uniform distribution of temperature along the wall. The materials of micro-emitter and shield are silicon carbide and the stainless steel	Fuel type: C_3H_8 (ER = 1.0) PV cells: GaSb Output power: 2.35 W
Yang et al. [26]	SiC porous medium foam is employed in a micro modular combustor. The porous medium can enhance heat transfer between the hot gas and the wall. Therefore, packing the micro-combustor with SiC porous media is an effective method to increase the wall temperature, subsequently increasing the radiation energy of the micro-TPV system	Fuel type: H_2 (ER = 1.0) PV cells: GaSb/InGaAsSb Output power: 13.1 W/6.1 W

methane–air mixture was delivered to the outer chamber of the micro-TPV reactor to sustain flame luminosity. By installing the micro-TPV reactor within a GaSb cell array, the effective power efficiency and overall efficiency of the micro-TPV power system were measured under various system configurations. The system was configured with extra components, such as a metal oxide–deposited layer on the quartz tube, a recirculating cap, and a reflecting mirror. The most relevant results are listed as follows:

1. Igniting the catalytic methane combustion over the platinum surface is difficult because of its lower chemical reactivity to platinum. Therefore, this study employed hydrogen in the inner chamber to induce the methane gas phase reaction in the outer chamber. Because of the high diffusion capacity of hydrogen, the heat and radicals were delivered to the other chamber through the perforations; in this manner, the methane chemical reaction was successfully initiated. Therefore, the methane hydrogen–air combustion maintained stable combustion inside the micro-TPV reactor.
2. The metal oxide–deposited quartz emitter heated up more easily to emit the radiation because of its high thermal conductivity, which is related to that of conventional silicon carbide. However, a large difference between the experimental results and the expectations ensued. The metal-oxide particles that had adhered on the inner surface of the quartz tube absorbed most of the radiation from the combustion, which led to a reduction of irradiance.
3. The effective power efficiency of the TPV system was only 3.24% when $ER_{in\text{-}H_2} = 0.7$ and $ER_{out\text{-}CH_4} = 0.9$. With a mirror and a recirculating tube, effective power efficiency was enhanced to 6.32%. To further improve the power efficiency of the micro-TPV reactor, an increase in radiant surface area of the micro-TPV reactor is necessary. Converting more thermal energy from the chemical exothermicity to radiant energy is a plausible solution to reduce energy waste and leverage the overall power efficiency of this micro-TPV system.

References

[1] Ferrari C, Melino F, Pinelli M, Spina PR. Thermophotovoltaic energy conversion: analytical aspects, prototypes and experiences. Appl Energy 2014;113:1717–30.
[2] Murugan S, Horák B. A review of micro combined heat and power systems for residential applications. Renew Sustain Energy Rev 2016;64:144–62.
[3] Qiu K, Hayden ACS. Implementation of a TPV integrated boiler for micro-CHP in residential buildings. Appl Energy 2014;134:143–9.
[4] Dunn-Rankin D, Leal EM, Walther DC. Personal power systems. Prog Energy Combust Sci 2005;31:422–65.
[5] Epstein AH. Millimeter-scale micro-electro-mechanical systems gas turbine engines. J Eng Gas Turb Power 2004;126:205–26.
[6] Aichlmayr HT, Kittelson DB, Zachariah MR. Micro-HCCI combustion: experimental characterization and development of a detailed chemical kinetic model with coupled piston motion. Combust Flame 2003;135:227–48.
[7] Qiu K, Hayden ACS. Development of a novel cascading TPV and TE power generation system. Appl Energy 2012;91:304–8.
[8] Yadav S, Yamasani P, Kumar S. Experimental studies on a micro power generator using thermo-electric modules mounted on a micro-combustor. Energy Convers Manage 2015;99:1–7.
[9] Wu Y-T, Li Y-H. Combustion characteristics of a micro segment platinum tubular reactor with a gap. Chem Eng J 2016;304:485–92.
[10] Yang WM, Chou SK, Shu C, Li ZW, Xue H. Combustion in micro-cylindrical combustors with and without a backward facing step. Appl Therm Eng 2002;22:1777–87.
[11] Chou SK, Yang WM, Chua KJ, Li J, Zhang KL. Development of micro power generators – a review. Appl Energy 2011;88:1–16.
[12] Bitnar B, Durisch W, Holzner R. Thermophotovoltaics on the move to applications. Appl Energy 2013;105:430–8.
[13] Gieras JF. Generators for portable power applications, advancements in electric machines. Netherlands, Dordrecht: Springer; 2008. p. 157–69.
[14] Yang WM, Chua KJ, Pan JF, Jiang DY, An H. Development of micro-thermo-photovoltaic power generator with heat recuperation. Energy Convers Manage 2014;78:81–7.
[15] Akhtar S, Kurnia JC, Shamim T. A three-dimensional computational model of H2–air premixed combustion in non-circular micro-channels for a thermo-photovoltaic (TPV) application. Appl Energy 2015;152:47–57.
[16] Kim NI, Kato S, Kataoka T, Yokomori T, Maruyama S, Fujimori T, Maruta K. Flame stabilization and emission of small Swiss-roll combustors as heaters. Combust Flame 2005;141:229–40.
[17] Ahn J, Eastwood C, Sitzki L, Ronney PD. Gas-phase and catalytic combustion in heat-recirculating burners. Proc Combust Inst 2005;30:2463–72.
[18] Zuo W, Jiaqiang E, Peng Q, Zhao X, Zhang Z. Numerical investigations on a comparison between counterflow and coflow double-channel micro combustors for micro-thermophotovoltaic system. Energy 2017;122:408–19.
[19] Mujeebu MA, Abdullah MZ, Bakar MZA, Mohamad AA, Abdullah MK. Applications of porous media combustion technology – a review. Appl Energy 2009;86:1365–75.
[20] Li Y-H, Chen G-B, Wu F-H, Cheng T-S, Chao Y-C. Effects of catalyst segmentation with cavities on combustion enhancement of blended fuels in a micro channel. Combust Flame 2012;159:1644–51.
[21] Maruta K, Takeda K, Ahn J, Borer K, Sitzki L, Ronney PD, Deutschmann O. Proceedings of the combustion instituteextinction limits of catalytic combustion in microchannels. Proc Combust Inst 2002;29:957–63.
[22] Lu Q, Pan J, Hu S, Tang A, Shao X. Hetero-/homogeneous combustion of premixed hydrogen–oxygen mixture in a micro-reactor with catalyst segmentation. Int J Hydrogen Energy 2016;41:12387–96.
[23] Su Y, Song J, Chai J, Cheng Q, Luo Z, Lou C, Fu P. Numerical investigation of a novel micro combustor with double-cavity for micro-thermophotovoltaic system. Energy Convers Manage 2015;106:173–80.
[24] Yang WM, Chou SK, Shu C, Li ZW, Xue H. Study of catalytic combustion and its effect on microthermophotovoltaic power generators. J Phys D Appl Phys 2005;38:4252.
[25] Yang W, Chou S, Chua K, An H, Karthikeyan K, Zhao X. An advanced micro modular combustor-radiator with heat recuperation for micro-TPV system application. Appl Energy 2012;97:749–53.
[26] Lee KH, Kwon OC. Studies on a heat-recirculating microemitter for a micro thermophotovoltaic system. Combust Flame 2008;153:161–72.
[27] Park JH, Lee SI, Wu H, Kwon OC. Thermophotovoltaic power conversion from a heat-recirculating micro-emitter. Int J Heat Mass Transf 2012;55:4878–85.
[28] Alipoor A, Saidi MH. Numerical study of hydrogen-air combustion characteristics in a novel micro-thermophotovoltaic power generator. Appl Energy 2017;199:382–99.
[29] Amano T, Yamaguchi M. Analysis of energy balance of electricity and heat generated by TPV generators. Sol Energy Mater Sol Cells 2001;66:579–83.
[30] Bitnar B, Durisch W, Mayor JC, Sigg H, Tschudi HR. Characterisation of rare earth selective emitters for thermophotovoltaic applications. Sol Energy Mater Sol Cells 2002;73:221–34.
[31] Daneshvar H, Prinja R, Kherani NP. Thermophotovoltaics: Fundamentals,

challenges and prospects. Appl Energy 2015;159:560–75.
[32] Yang WM, Chou SK, Chua KJ, Li J, Zhao X. Research on modular micro combustor-radiator with and without porous media. Chem Eng J 2011;168:799–802.
[33] Wu H, Kaviany M, Kwon OC. Thermophotovoltaic power conversion using a superadiabatic radiant burner. Appl Energy 2017. http://dx.doi.org/10.1016/j.apenergy.2017.08.168.
[34] Yang WM, Chou SK, Shu C, Li ZW, Xue H. Experimental study of micro-thermophotovoltaic systems with different combustor configurations. Energy Convers Manage 2007;48:1238–44.
[35] Su Y, Cheng Q, Song J, Si M. Numerical study on a multiple-channel micro combustor for a micro-thermophotovoltaic system. Energy Convers Manage 2016;120:197–205.
[36] Qiu K, Hayden ACS. Direct thermal to electrical energy conversion using very low bandgap TPV cells in a gas-fired furnace system. Energy Convers Manage 2014;79:54–8.
[37] Park JH, So JS, Moon HJ, Kwon OC. Measured and predicted performance of a micro-thermophotovoltaic device with a heat-recirculating micro-emitter. Int J Heat Mass Transf 2011;54:1046–54.
[38] Deutschmann O, Schmidt R, Behrendt F, Warnat J. Numerical modeling of catalytic ignition. Symp (Int) Combust 1996;26:1747–54.
[39] Li Y-H, Chen G-B, Wu F-H, Cheng T-S, Chao Y-C. Combustion characteristics in a small-scale reactor with catalyst segmentation and cavities. Proc Combust Inst 2013;34:2253–9.
[40] Li Y-H, Chen G-B, Cheng T-S, Yeh Y-L, Chao Y-C. Combustion characteristics of a small-scale combustor with a percolated platinum emitter tube for thermophotovoltaics. Energy 2013;61:150–7.
[41] Cheng TS, Wu CY, Chen CP, Li YH, Chao YC, Yuan T, Leu TS. Detailed measurement and assessment of laminar hydrogen jet diffusion flames. Combust Flame 2006;146:268–82.
[42] Reinke M, Mantzaras J, Bombach R, Schenker S, Inauen A. Gas phase chemistry in catalytic combustion of methane/air mixtures over platinum at pressures of 1 to 16 bar. Combust Flame 2005;141:448–68.
[43] Karagiannidis S, Mantzaras J. Numerical investigation on the hydrogen-assisted start-up of methane-fueled, catalytic microreactors. Flow Turbul Combust 2012;89:215–30.
[44] Argyle MD, Bartholomew CH. Heterogeneous catalyst deactivation and regeneration: a review. Catalysts 2015;5:145–269.